NANO LETTERS

Letter

pubs.acs.org/NanoLett

Ion Implantation of Graphene—Toward IC Compatible Technologies

U. Bangert,*[,†] W. Pierce,[†] D. M. Kepaptsoglou,[‡] Q. Ramasse,[‡] R. Zan,[†] M. H. Gass,[‡,§] J. A. Van den Berg,[∥] C. B. Boothroyd,[⊥] J. Amani,[#] and H. Hofsäss[#]

[†]School of Materials, The University of Manchester, Manchester M13 9PL, United Kingdom

[‡]SuperSTEM Laboratory, STFC Daresbury Campus, Daresbury WA4 4AD, United Kingdom

[§]AMEC, Walton House, 404 The Quadrant, Birchwood, WA3 6GA, United Kingdom

[∥]School of Computing, Science and Engineering, University of Salford, Salford, Greater Manchester M5 4WT, United Kingdom

[⊥]Ernst Ruska-Centre for Microscopy and Spectroscopy with Electrons and Peter Gruenberg Institute, Juelich Research Centre, D-52425 Juelich, Germany

[#]II. Physikalisches Institut, Georg-August-Universität Göttingen, Friedrich-Hund-Platz 1, 37077 Göttingen, Germany

ABSTRACT: Doping of graphene via low energy ion implantation could open possibilities for fabrication of nanometer-scale patterned graphene-based devices as well as for graphene functionalization compatible with large-scale integrated semiconductor technology. Using advanced electron microscopy/spectroscopy methods, we show for the first time directly that graphene can be doped with B and N via ion implantation and that the retention is in good agreement with predictions from calculation-based literature values. Atomic resolution high-angle dark field imaging (HAADF) combined with single-atom electron energy loss (EEL) spectroscopy reveals that for sufficiently low implantation energies ions are predominantly substitutionally incorporated into the graphene lattice with a very small fraction residing in defect-related sites.

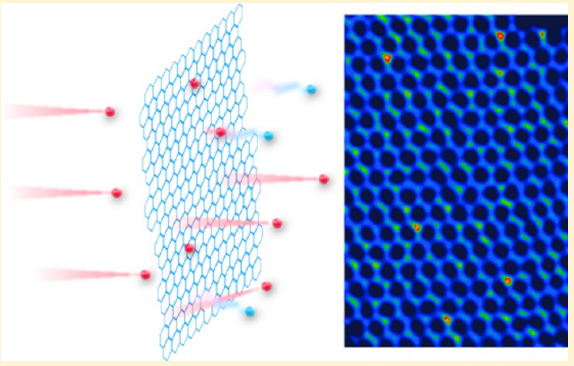

KEYWORDS: *Graphene, doping, ion implantation, STEM, EELS*

Despite its outstanding properties such as high transparency, high carrier mobility (150 000 $cm^2/(V\ s)$), ballistic transport,[1] thermal conductivity,[2] and mechanical strength,[3] graphene's potential for device applications is severely infringed due to the lack of a bandgap leading to poor on/off ratios. Measures such as reducing its dimensions (graphene nanoribbons and nanodots)[4] result in the opening of a bandgap,[5,6] as does the introduction of adatoms, defects (although this might worsen the high mobilities),[7] or the application of an electric field.[8] Bandstructure tailoring through electronic doping other than electric gauging or chemical functionalization would be a major breakthrough. Chemical methods have significant drawbacks due to lack of control, contamination and inferred secondary impurities, instability, and site selectivity. Although successful n-doping with N via the chemical route and subsequent annealing has been reported[9] and N-dopants have been visualized via high-resolution transmission electron microscopy,[10,11] introducing dopants directly into the lattice in a controlled, pristine fashion via low-energy ion implantation is highly desirable.

Ion implantation, by enabling flexible small-depth channel doping, has revolutionized Si- and generally semiconductor-technology with a most significant economic and societal impact. Integration of graphene into these technologies will be a further and major step-up. If ion implantation of graphene with, for example, N and B was proven to be successful, industrial implantation facilities could be refitted with low energy implantation capabilities, and thus, having control over ion energies and conceivably using focused ion beams, one could envisage fabrication of spatially nonuniform graphene-based materials where N- and B-doped areas can be made. This presents huge prospect for industrial scale, nonchemistry reliant functionalization and processing of 2D materials.

Concerning irradiation assisted graphene doping there have been reports of introducing substitutional dopants via a two-step process by combining high energy irradiation to form vacancies with deposition of metals to fill the holes.[12] There is also ample literature on modeling of the effects of ion-irradiation in graphene (e.g., ref 13) as well as defect studies at higher irradiation energies. More recently, density functional theory calculations have focused on low energy ion implantation of graphene. Åhlgren et al.[14] predict that the optimum irradiation energy of 50 eV leads to substitution probabilities of 55% for N. Combining this with classical MD simulations the authors found that the probability for creating other defects is close to 30−50%. Furthermore the authors also report that by lowering the implantation energy below the

Received: July 28, 2013
Revised: September 17, 2013
Published: September 23, 2013

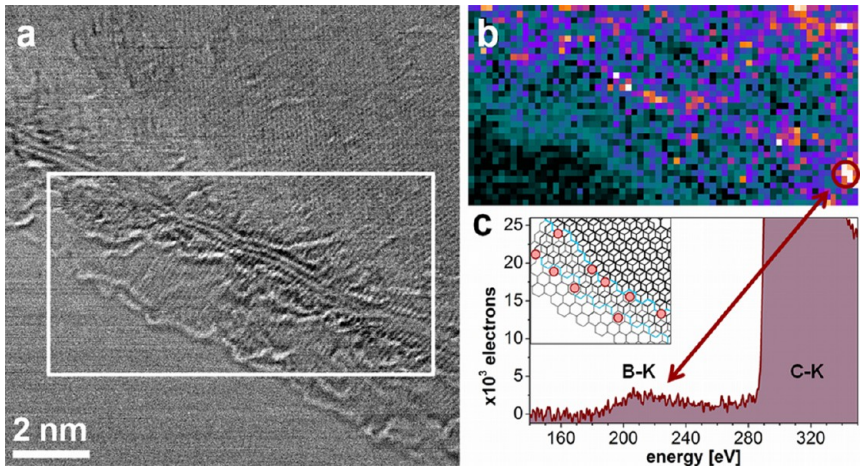

Figure 1. (a) High-resolution SuperSTEM BF image of staggered graphene sheets; leftmost is a single layer, followed toward the right by a second sheet with a rough edge, which, in turn, is followed by further few graphene sheets with partially straight edges. The sample was implanted at 100 eV with B to a dose of 10^{14} cm^{-2}. The white frame denotes an area in which an EEL spectrum image was taken. (b) Color map of the signal intensity in the energy regime of the B−K-edge (190−230 eV) extracted from an SI consisting of 65 × 33 pixels with pixel size 0.14 × 0.14 nm^2 (assigning ∼one atom to each pixel). Pixels where the B−K edge signal is significantly (∼3×) above the noise band are red/yellow/white. (c) EEL spectrum showing the B−K-edge, extracted from a 2 × 2 pixel area denoted by the red circle indicated by the arrow. The B-signal distribution suggests that single B-atoms and few atom clusters thereof have attached to sheet edges or to monatomic steps as depicted in the sketch in part c.

threshold for creating single vacancies, the vacancies created while doping can be filled by further dopant atoms to reach a significantly higher substitution-to-defect ratio. The above reports of substitutional N-doping of graphene and defect site formation resulting from low energy ion implantation have yet to be verified unambiguously via imaging and spectroscopy of such implants. Very recent experiments carried out by one of the authors of the present article[15] on low energy B- and N-implantation followed by characterization via X-ray photoelectron spectroscopy (XPS) and Raman showed that graphene can indeed be doped under incorporation of N into the graphene lattice and that damage is introduced, but to a much lesser extent than with higher implantation energies (the results from accompanying calculations are referred to in the Methods section). Again, direct evidence of sites and distribution of individual dopants is lacking. The combination of electron microscopy and electron energy loss (EEL) spectroscopy can provide not only information about the nature and site of an individual impurity atom, but also about its bonding state.[16] EEL spectroscopy in conjunction with lattice imaging has previously been applied to study the mechanism of electron beam damage in an electron microscope (typically at energies >100 keV) in nitrogen-doped graphene and carbon nanotubes,[17] but as yet there has been no assessment by electron microscopy (with e-beam energies below the carbon displacement threshold) of low energy ion-doped graphene.

Here we report on B- and N-ion implantation of free-standing graphene with ion energies from 200 down to 20 eV, and on imaging and EEL spectroscopy measurements in aberration corrected transmission electron microscopes with e-beam energies of 80 down to 60 keV (see Methods section). For the case of 200 eV N-implanted samples the overall N-retentions range from ∼5 to 15% of the implanted dose. It should be noted that EEL spectra were obtained from areas of the order of 1000 nm^2, including ubiquitous contamination. For the 100 eV B-implanted samples the retention rose to 50%; again the measurements included contaminated areas. In largely contamination free areas the retention was significantly less, of the order of 15%. We investigated pristine graphene areas in detail via EEL spectrum imaging carried out in a dedicated scanning transmission electron microscope (STEM). The area shown in Figure 1a consists of staggered graphene sheets with a single sheet protruding at the sample edge. The composition map highlights B-atom signals by red/yellow/white pixels (Figure 1b). The position of these signals was derived from the integrated intensity of the EEL signal in the energy range 190−230 eV (Figure 1c). Red/yellow/white pixels have B−K-edge signals, and the yellow/white colors indicate signals 3× higher than the noise band. The pixel size of the spectral map is 0.14 nm × 0.14 nm; hence each pixel encompasses the area of an atom. B-atoms are seen along edges of the graphene sheets and at creases. The EEL absorption edge in contamination-free areas is lacking the π^* peak in the energy region 192−195 eV (Figure 1c) in contrast to large-area B-EEL spectra; this feature is commonly ascribed to B−O-, B−N-, or pyridinic bonds of B in carbon nanostructures.[18−20] The question remains how and if ions implanted at energies ≥100 eV are incorporated into the graphene lattice. The observations in Figure 1 suggest that the majority of implants in clean patches attach to defect states like graphene edges. Further atomic resolution HAADF imaging combined with atomic resolution EEL spectroscopy (see below for details) of samples implanted as above did not reveal implanted ions residing in the pristine graphene lattice. It can thus be assumed that ions penetrate pristine graphene at energies ≥100 eV and are only retained in "thicker" regions, that is, in contamination and at graphene edges in multilayers, as well as in the multilayers themselves,[20] like in the region in the right-hand top corner of the white-framed box in Figure 1a.

To ensure ion incorporation, a lower implantation energy of 25 eV, as theoretically discussed,[14] has been employed, and a combined high-resolution STEM and EEL study of atomically clean graphene has been carried out. This proves the Åhlgren[14] predictions, namely, incorporation of ions into graphene lattice sites with minimum damage (substitutional or in ion-vacancy complexes) for the case of N ions implanted at energies <50 eV. Due to its $\sim Z^2$ contrast dependency, HAADF imaging is ideally suited for visualization of foreign elements in single graphene layers. Although B is only one element down and N is

dx.doi.org/10.1021/nl402812y | Nano Lett. 2013, 13, 4902−4907

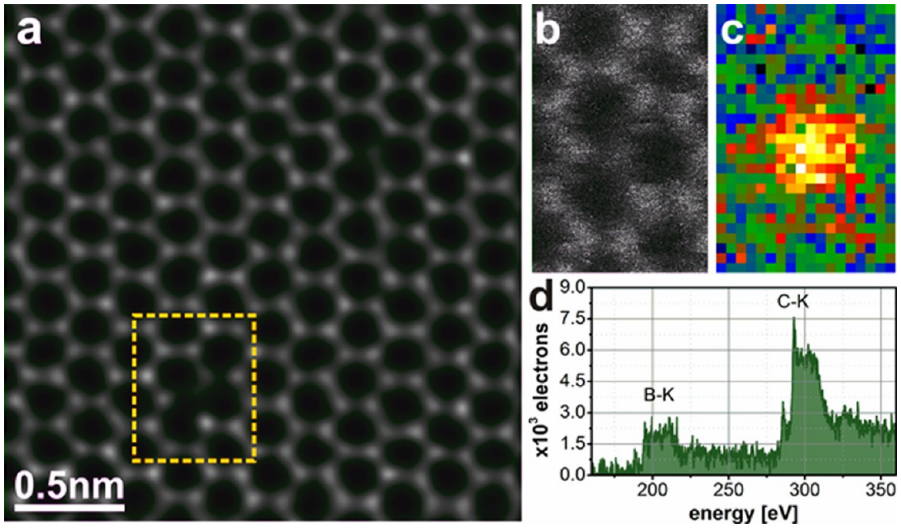

Figure 2. (a) Double Gaussian filtered atomic resolution HAADF image of a substitutional B-atom in graphene (for process details see Methods section); (b) raw HAADF signal obtained from the framed area in (a) simultaneously with the EEL spectrum image in c. The B-atom can be seen to have a lower intensity than the C-atoms, according to the Z^2 intensity relationship in HAADF images; (c) EEL spectrum image intensity in an energy window (190−220 eV) around the N−K edge, representing an atomic boron map ("temperature" color scale, blue/green: low intensity, yellow/white: high intensity); (d) sum of spectra extracted from pixels of the spectrum image represented in part d of the area around and including the B-atom.

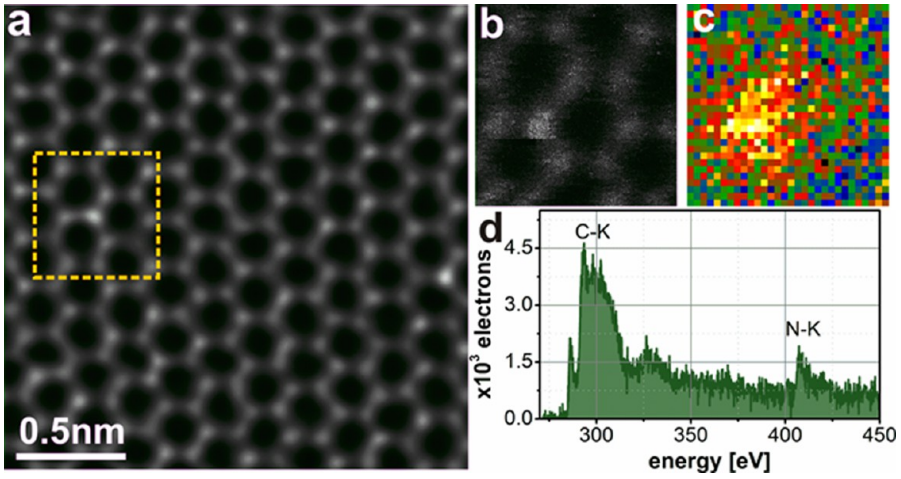

Figure 3. (a) Double Gaussian filtered atomic resolution HAADF image of a substitutional N-atom in graphene (for process details see Methods section); (b) raw HAADF signal obtained from the framed area in part a simultaneously with the EEL spectrum image in c. The N-atom can be seen to have higher intensity than the C-atoms, according to the Z^2 intensity relationship in HAADF images; (c) EEL spectrum image intensity in an energy window (400−420 eV) around the N−K edge, representing an atomic boron map ("temperature" color scale, blue/green: low intensity, yellow/white: high intensity); (d) sum of spectra extracted from pixels of the spectrum image represented in d of the area around and including the N-atom.

one element up from C in the periodic table, the contrast ratios should scale as 25:36 and 49:36, respectively; hence B should be ∼30% darker and N ∼36% brighter than C. This is indeed observed in Figure 2a,b for B and in Figure 3a,b for N in pristine graphene patches. The respective EEL spectra (Figures 2d and 3d) undoubtedly confirm the presence of a B and an N atom in the graphene lattice. Individual substitutional incorporation of B atoms directly into the graphene lattice has not been demonstrated until now. P-doping has so far only been reported via adsorbates (e.g., ref 21) or charge transfer between graphene and a substrate.[22−24] The achievement reported in this article is the success with controlled, direct substitutional, extrinsic p-doping, which adds significant flexibility to the use in and fabrication of electronic components. Furthermore the implanted ions appear to be stable as evidenced from repeated STEM scans, during which both N and B remained in identical lattice positions. In the following we present more detailed results of N-implants. We found that the overall retention (over a total investigated area of ∼1000 nm^2) rose to 100% for the 25 eV implantation energy; however, when focusing on pristine graphene patches, a retention of only ∼15% was measured. This suggests that the large majority of implants reside within/underneath graphene's surface contamination. The reason for this might be that the surface contamination, presenting a thicker than monolayer target, results in more ions being stopped.

Contrast profiles taken along rows of C-atoms, containing an N atom, agree extremely well with the above expectations from

dx.doi.org/10.1021/nl402812y | Nano Lett. 2013, 13, 4902−4907

HAADF intensity ratios. Intensity distribution statistics for N were obtained from a number (~12) atomic resolution HAADF images, like the one shown in Figures 3a and 4a.

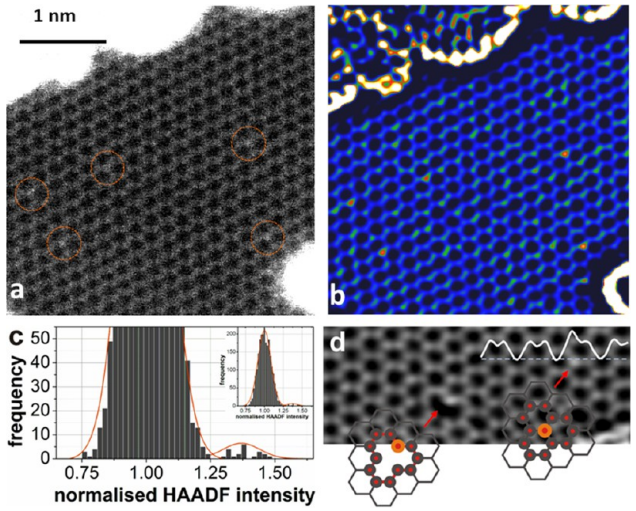

Figure 4. Atomic resolution HAADF image of graphene implanted at 25 eV with N to a dose of 2×10^{14} cm^{-2} (a) showing raw data and (b) obtained by deconvolution of image a as described in the text. The patches in the top left and bottom right corners are ubiquitous contamination; N-atoms (here all substitutional) show up as brighter contrast spots (encircled) in a and as orange spots in the false color image in b, where colors are assigned on a temperature scale with increasing intensity represented by the color sequence ranging from blue (thin regions or low atomic number) over orange to yellow/white (thick regions or high atomic number); (c) intensity histogram of C- and N-atoms, the latter having intensity values >2σ larger than C-atoms (set at the value of 1); (d) pristine graphene patch (deconvolved image as in b) with an N-atom adjacent to a vacancy and a substitutional N-atom. Model sketches are shown below. An intensity trace along the dotted line is overlaid on image d, showing the expected 1.4× enhancement at the N-atom.

Additionally EEL spectra were acquired from individual N-atoms, and HAADF images of the EEL spectrum image region are taken simultaneously with the EEL acquisition (Figure 3b and c). The N−K-edge was always observed in EEL spectra extracted from regions at/on N-atoms in the spectrum images (Figure 3d).

To obtain N-concentrations, the intensity profiles of atoms in a number of HAADF images (amounting to several thousand atoms) were obtained and plotted as histograms. This was done in various ways including line profiling and using an algorithm that locates the maxima in a small region centered on each atom (see Methods section for details). Plotting the data on a histogram the C-atom distributions in all HAADF images showed a consistently similar Gaussian distribution and a clear separation of the nitrogen "outliers" (see Figure 4c). Peak fitting of the histogram with a Gaussian curve gave a peak center of 0.9492 and σ = 0.1323 (±14% spread around the center). If the criterion for the existence of a nitrogen atom is given by its intensity position being more than 2σ remote (toward the higher end of the scale) from the carbon peak intensity position, we find there are five nitrogen atoms in a total of ~530 carbon atoms in the image in Figure 4a. This represents a doping level of around 1% and agrees well with visual inspection, where the five possible nitrogen atoms are significantly brighter than their surrounding carbon atoms. The image intensity increase measured at these atoms yields an intensity ratio $I_{nitrogen}/I_{carbon}$ of 1.3−1.5—so N-atoms are ~30−50% brighter than C-atoms—which complies well with that of 1.36 from Z^2 ratios. Fully automated detection of the peaks gives similar results with σ = 0.1167 and the center at 0.9969 resulting in a similar doping level of around 1%. Atoms with an intensity larger than 2 σ of that of the center have been labeled in Figure 4a and b. An example of the intensity difference of N- and C-atoms is shown in the overlaid HAADF intensity profile in Figure 4d; it was taken along the underlying dashed line. The N-concentration in this particular area is 0.5%. This is significantly lower than predicted; however, the average concentration of ~1% of many clean graphene patches is in better agreement with the predicted 5%. The fact that the N-distribution is nonuniform is surprising and requires further investigation; shielding and deflection of the low energy ion-beam due to charging of the contamination could play a role, as well as preferential incorporation in defected or contaminated regions, for example, at vacancies, edges, and adatoms. A number of N-atoms have been observed at sites of vacancy defects. An example is shown in Figure 4d where a nitrogen atom sits at the edge bordering a vacancy defect. Such defects, however, are not stable in repeated scans in the STEM; hence it is questionable, whether they have formed with e-beam assistance at N-sites in the first place. The overall defect concentration is <1% of the original implantation dose and less than 10% of the retained N-fraction. The large majority of implanted N-atoms was observed in substitutional sites. This may prove the predictions by Åhlgren et al.[14] that, by lowering the implantation energy, the vacancies created while doping can be eliminated via subsequent filling with dopant atoms and thus reach a significantly higher substitution-to-defect ratio.

In conclusion we have shown via atomic resolution imaging and nanoscale EEL spectroscopy, which in the new generation dedicated STEMs can be carried out at the single-atom level, that B and N can be implanted into graphene. Aside from incorporation into surface artifacts/contamination it was found that at implantation energies between 100 and 200 eV ion retention in pristine graphene occurs mainly within few-layer patches and at edges of staggered sheets, but not notably in single layers. At energies below 50 eV, however, ion-implantation deposits atoms in single layer graphene. Direct observations of individual N- and B-atoms via atomic resolution HAADF and single-atom EEL spectroscopy proved incorporation of these dopants into the graphene lattice. Statistical evaluation in the case of N showed an average retention of ~16% with over 90% of this retention constituting substitutional nitrogen. Whereas successful n-type doping of graphene with nitrogen, albeit via chemical methods, has been suggested in the literature, extrinsic substitutional p-type doping is currently still questionable. We provide direct proof that this is possible with boron. Importantly, both B- and N-doping can be achieved via nonchemical processes used in commercial semiconductor technologies. Although the electronic properties resulting from the ion implantation need to be further investigated, our results demonstrate that ion implantation shows huge prospects for large-scale controlled and flexible doping of graphene and, generally 2D materials, providing a method compatible with those in IC technologies.

Methods. Ion implantations of N and B were carried out at the implanters at the Surrey University Ion Beam Centre (200 eV), at the Salford University low energy implantation facility (100 eV; base pressure ~2−3 × 10^{-8} Pa), and at the Göttingen

dx.doi.org/10.1021/nl402812y | Nano Lett. 2013, 13, 4902−4907

mass selected ion beam deposition system (25 eV), routinely used for low energy ion beam deposition of diamond-like thin films.[25,26] To achieve the ultralow energies in the latter system, a 30 keV mass selected $^{14}N^+$ ion beam is decelerated toward the graphene target down to an energy of 25 eV. Before deceleration, the beam is deflected to eliminate possible neutralized ions, and a beam sweep ensures a uniform profile over an area of 1.5 cm^2. The deceleration bias voltage is set relative to the ion source anode potential, so that 25 eV is the maximum ion energy with a few electron volts wide tail toward lower energies. The vacuum during irradiation was 2×10^{-6} Pa. Graphene layers on TEM grids were irradiated at room temperature and a fluence of $(2 \pm 1) \times 10^{14}$ cm^{-2}. The uncertainty arises because the beam size after deceleration is not precisely known.

The implantation process into graphene was simulated with the Monte Carlo program SDTrimSP,[27] which is designed for atomic collisions in amorphous targets in particular to calculate low energy processes such as sputtering. We simulated ion impact on an amorphous carbon layer of 3×10^{15} atoms/cm^2 (the atomic areal density of a single graphene layer) and perpendicular ion incidence. A C-atom is ejected from the layer if its recoil energy component perpendicular to the layer exceeds a typical surface binding energy of ~7.4 eV. For N-ions possessing an energy of 25 eV about 50% of the ions should remove a C-atom and will be incorporated into the sheet; the rest is transmitted. For an implantation fluence of $(2 \pm 1) \times 10^{14}$ cm^{-2} this means that approximately 1.5−5% of the C-atoms should be exchanged by N-atoms. This is somewhat higher compared to our observations of an N-atom content of around 1%. One reason for the discrepancy may be the regular graphene structure compared to the amorphous layer in the simulation. Also shielding and deflection of the N ions due to surface contaminations may play a role.

Microscopy images and electron energy loss (EEL) spectra were acquired at the SuperSTEM Laboratory on Nion (VG HB501, retroffited with a Nion aberration corrector and UltraSTEM100) dedicated ultrahigh vacuum scanning transmission electron microscopes[28] equipped with cold field emission guns with a native energy spread of 0.3−0.35 eV and operated at 80 keV (VG HB501) and 60 keV (UltraSTEM) to prevent knock-on damage to the graphene samples. Additional energy filtered imaging and EEL spectroscopy was carried out on a triple aberration-corrected, monochromated TitanPICO at 80 keV in the Ernst Ruska Centre, Juelich. For atomic resolution high angle annular dark field (HAADF) imaging on the Daresbury SuperSTEM instruments the estimated probe size (full width at half-maximum) was 1.2 Å. The HAADF detector used to record the *Z*-contrast images had inner and outer radii of 86 and 190 mrad, respectively: in these conditions, the intensity recorded with the probe positioned on an atomic site is approximately proportional to the square of the average atomic number *Z* of this site.[29] EEL spectra and spectrum images of subnanometer areas surrounding few atoms were recorded with a Gatan Enfina spectrometer; spectra of larger areas following observations at the TitanPICO were obtained with a Quantum Gatan Imaging filter.

HAADF images were processed using a double Gaussian filtering routine as described by Krivanek et al.[30,31] In our case the fwhm of the inner Gaussian was adjusted per image with a typical fwhm of 0.8 Å and that of the "tail" Gaussian to approximately double this width. The intention of this procedure is to remove intensity effects of the e-beam probe tail from the center of the benzene rings, so that these possess the intensity of empty space, that is, the background intensity.

AUTHOR INFORMATION

Author Contributions

U.B. conceived the project and guided the measurements. D.M.K., M.H.G., and Q.R. carried out SuperSTEM measurements, and C.B.B. carried out measurements on the TitanPICO. W.P. wrote and applied routines for data evaluation. R.Z. provided the graphene TEM samples. J.A.V. performed ion implantations at 100−200 eV, and J.A. and H.H. performed ultra low energy ion implantation and Monte Carlo calculations. U.B. wrote the manuscript, and U.B. and D.M.K. prepared the figures. All authors discussed the results and commented on the manuscript.

Notes

The authors declare no competing financial interest.

ACKNOWLEDGMENTS

We acknowledge R. Gwilliam for overseeing the ion implantations in the Surrey Ion Beam Centre and EPSRC for funding the project through grant EP/I008144/1 and for support of the SuperSTEM National Facility of Aberration Corrected STEM.

REFERENCES

(1) Geim, A. K.; Novoselov, K. S. *Nat. Mater.* **2007**, *6*, 183.
(2) Balandin, A. A.; Gosh, S.; Bao, W.; Calizo, I.; Teweldebrhan, D.; Miao, F.; Lau, C. N. *Nano Lett.* **2008**, *8*, 902.
(3) Lee, C.; Wei, X.; Kysar, J. W.; Hone, J. *Science* **2008**, *321*, 385.
(4) Novoselov, K. S.; Falko, V. I.; Colombo, L.; Gellert, P. R.; Schwab, M. G.; Kim, K. *Nature* **2012**, *490*, 192.
(5) Han, M. Y.; Ozyilmaz, B.; Zhang, Y.; Kim, P. *Phys. Rev. Lett.* **2007**, *98*, 206804.
(6) Son, Y. W.; Cohen, M. L.; Louie, S. G. *Phys. Rev. Lett.* **2006**, *97*, 216803.
(7) Wehling, T. O.; Katnelson, M. I.; Lichtenstein, A. I. *Phys. Rev. B* **2009**, *80*, 085428.
(8) Ohta, T.; Bostwick, A.; Seyller, T.; Horn, K.; Rotenberg, E. *Science* **2006**, *313*, 951.
(9) Meyer, J. C.; et al. *Nat. Mater.* **2011**, *10*, 209.
(10) Zhao, L.; et al. *Science* **2011**, *333*, 999.
(11) Huo, B.; Liu, Q.; Chen, E.; Zhu, H.; Pang, L.; Gong, J. R. *Nano Lett.* **2010**, *10* (12), 4975.
(12) Wang, H.; Wang, Q.; Cheng, Y. C.; Li, K.; Yao, Y.; Zhang, Q.; Dong, C.; Wang, P.; Schwingenschlögl, U.; Yang, W.; Zhang, X. X. *Nano Lett.* **2012**, *12*, 141.
(13) Lehtinen, O.; Kotakoski, J.; Krasheninnikov, A. V.; Tolvanen, A.; Nordlund, K.; Keinonen, J. *Phys. Rev. B* **2010**, *81*, 153401.
(14) Ahlgren, E. H.; Kotakovski, J.; Krasheninnikov, A. V. *Phys. Rev. B* **2011**, *83*, 115424.
(15) Xu, Y.; Zhang, K.; Brüsewitz, C.; Wu, X.; Hofsäss, H. *AIP Adv.* **2013**, *3*, 072120.
(16) Ramasse, Q. M.; Seabourne, C. R.; Kepaptsoglou, D.-M.; Zan, R.; Bangert, U.; Scott, A. J. *Nano Lett.* **2012**, No. 10.1021/nl304187e.
(17) Susi, T.; Kotakoski, J.; Arenal, R.; Kurasch, S.; Jiang, H.; Skakalova, V.; Stephan, O.; Krasheninnikov, A. V.; Kauppinen, E. I.; Kaiser, U.; Meyer, J. C. *ACS Nano* **2012**, *6* (10), 8837.
(18) Gai, P. L.; Stéphan, O.; McGuire, K.; Rao, A. M.; Dresselhaus, M. S.; Dresselhaus, G.; et al. *J. Mater. Chem.* **2004**, *14*, 669.
(19) Arenal, R.; de la Pena, F.; Stéphan, O.; Walls, M.; Tence, M.; Loiseau, A.; et al. *Ultramicroscopy* **2008**, *109*, 32.
(20) Bangert, U.; Bleloch, A.; Gass, M. H.; Seepujak, A.; Van den Berg, J. *Phys. Rev. B* **2010**, *81*, 245423.
(21) Gierz, I.; Riedl, C.; Starke, U.; Ast, C. R.; Kern, K. *Nano Lett.* **2008**, *8* (12), 4603.

(22) Cheng, Y. C.; Schwingenschlögl, U. *Appl. Phys. Lett.* **2010**, *97*, 193304.
(23) Vinogradov, N. A.; Simonov, K. A.; Generalov, A. V.; Vinogradov, A. S.; Vyalikh, D. V.; Laubschat, C.; Mårtensson, N.; Preobrajenski, A. B. *J. Phys.: Condens. Matter* **2012**, *24*, 314202.
(24) Song, W.; Kim, Y.; Kim, S. H.; Kim, S. Y.; Cha, M.-J.; Song, I.; Jung, D. S.; Jeon, C.; Lim, T.; Lee, S.; Ju, S.; Choi, W. C.; Jung, M. W.; An, K.-S.; Park, C.-Y. *Appl. Phys. Lett.* **2013**, *102*, 053103.
(25) Hofsäss, H.; Binder, H.; Klumpp, T.; Recknagel, E. *Diam. Relat. Mater.* **1994**, *3*, 137.
(26) Hofsäss, H.; Ronning, C.; Feldermann, H. Proc. 16th Int Conf on the Application of Accelerators in Research and Industry, Denton, TX, USA, Nov 1−4, 2000; Duggan, J. L.; Lon Morgan, I., Eds. *AIP Conf. Proc.* **2001**, *576*, 947.
(27) Eckstein, W.; Dohmen, R.; Mutzke, A.; Schneider, R. *IPP Report 12/3*; Max Planck Institute for Plasma Physics: Greifswald, Germany, 2007.
(28) Krivanek, O. L.; Dellby, N.; Murfitt, M. F.; Chisholm, M.; Pennycook, T. J.; Suenaga, K.; Nicolosi, V. *Ultramicroscopy* **2010**, *110*, 935.
(29) Hartel, P.; Rose, H.; Dinges, C. *Ultramicroscopy* **1996**, *63*, 93.
(30) Krivanek, O. L.; Chisholm, M. F.; Nicolosi, V.; Pennycook, T. J.; Corbin, G. J.; Dellby, N.; Murfitt, M. F.; Own, C. S.; Szilagyi, Z. S.; Oxley, M. P.; Pantelides, S. T.; Stephen, J.; Pennycook, S. J. *Nature* **2010**, *464*, 571.
(31) Krivanek, O. L.; Chisholm, M. F.; Murfitt, M. F.; Dellby, N. *Ultramicroscopy* **2012**, *123*, 90.